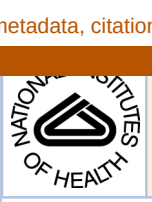

Published in final edited form as:

Bone. 2010 August ; 47(2): 241–247. doi:10.1016/j.bone.2010.05.016.

One Year of Alendronate Treatment Lowers Microstructural Stresses Associated with Trabecular Microdamage Initiation

Jessica M. O'Neal[a,b], **Tamim Diab**[a], **Matthew R. Allen**[c], **Brani Vidakovic**[f], **David B. Burr**[c,d,e], and **Robert E. Guldberg**[1]

[a] Parker H. Petit Institute for Bioengineering and Bioscience and George W. Woodruff School of Mechanical Engineering, Georgia Institute of Technology, Atlanta, GA, USA

[b] School of Medicine, Medical College of Georgia, Augusta, GA, USA

[c] Department of Anatomy and Cell Biology, Indiana University School of Medicine, Indianapolis, IN, USA

[d] Department of Orthopaedic Surgery, Indiana University School of Medicine, Indianapolis, IN, USA

[e] Department of Biomedical Engineering, Indiana University—Purdue University at Indianapolis, Indianapolis, IN, USA

[f] Wallace H. Coulter Department of Biomedical Engineering, Georgia Institute of Technology, Atlanta, GA, 30332 U.S.A

Keywords

Bisphosphonate; Bone quality; Finite Element Modeling; Microcomputed Tomography; Osteoporosis

1. Introduction

Alendronate, a bisphosphonate used to treat low bone density associated with osteoporosis, has been shown to decrease fracture risk at both vertebral and non-vertebral sites. [1–3] It achieves this risk reduction principally by increasing bone mineral density at the structural level. Positive effects at the tissue level may also improve fracture risk early in treatment by improving trabecular microarchitecture and reducing the number of trabecular stress risers (unfilled resorption pits) at sites of remodeling. [4] Studies conducted in canine models have shown, however, that one year of alendronate treatment is associated with decreased toughness and increased microcrack density, though these two findings may be the result of different mechanisms. [5] Furthermore, studies by Stepan *et. al*. found increased crack density in osteoporotic women using alendronate compared to treatment-naïve osteoporotic controls, whereas another study of osteoporotic women did not find significantly increased microdamage frequency compared to cadaver controls. [6,7] A better understanding of the

Corresponding author: Robert E. Guldberg, Ph.D., Institute for Bioengineering and Biosciences, 315 Ferst Drive, Atlanta, GA 30332-0405, robert.guldberg@me.gatech.edu, Phone: (404) 894-6589 Fax: (404) 385-1397.

mechanistic basis of damage formation with alendronate treatment can provide new insight into the underlying mechanisms of bone fragility.

Bone derives its ability to resist fracture by forming microdamage when subjected to loading. Traditionally, microdamage in trabecular bone has been grouped into two different morphological categories: linear microcracks and diffuse damage. Histologically, linear microcracks are identified as individual, sharply defined cracks, while diffuse damage is an of arrays of cracks. [8,9] It has been shown that different damage morphologies affect the biomechanical properties of bone differently [10–12]. Diffuse damage formation plays a significant role in prolonging the fatigue life of bone and resisting a catastrophic fracture. [10,11] In contrast, linear microcracks can reduce bone strength and stiffness and are traditionally associated with the terminal phase of fatigue fracture characterized by rapid crack propagation and catastrophic failure. [10,11] Severe damage (defined by Moore and Gibson as a primary crack with secondary cracks, or through-trabecular thickness cracks) also occurs at a later stage in the fracture process [13,14] Although microdamage accumulation has been documented with alendronate use, [6,7] its significance to bone fragility is still unknown.

We have previously reported a specimen-specific finite element technique to assess trabecular level stresses associated with microdamage initiation in bovine trabecular bone. [15,16] With this technique, the relationship between local damage events and trabecular stress magnitude can be directly assessed and associated with trabecular architectural characteristics. The overall goal of the study was to investigate whether changes in bone quality occurring after one year of alendronate treatment will result in an increased propensity to form microdamage. The specific objectives were to (a) quantify the von Mises stress state of trabeculae demonstrating different morphologies of damage and compare between alendronate-treated and control groups, and (b) to determine if changes in microarchitectural characteristics due to alendronate treatment are associated with damage morphology.

2. Materials and Methods

2.1 Animals

Detailed methods regarding alendronate administration for this study have been previously reported. [5] Briefly, one-year-old female beagle dogs were randomized into three groups and treated with oral doses of saline (1.0 mL/kg/day) or alendronate (ALN, 0.2 mg/kg/day or 1.0 mg/kg/day) for one year. The ALN 0.2 and ALN 1.0 doses approximate the clinical doses used for the treatment of postmenopausal osteoporosis and Paget's disease, respectively. The group treated with saline served as the control group. All procedures were approved by the Indiana University School of Medicine Animal Care and Use Committee.

2.2 Sample Extraction

Twelve right distal femurs from beagle dogs (n=4 in each treatment group) were obtained for analysis. One trabecular core from each specimen (diameter = 5 mm; length = 18 mm) was extracted by coring through the condyle of the distal femur in the approximate principal material direction using a trephine under constant irrigation with 0.9% physiological saline + 10 μmol/L protease inhibitor (E-64, Sigma Chemical) followed by sizing with a diamond saw. The protease inhibitor (PI) was used throughout the experiment to minimize tissue degradation. The specimens were wrapped in saline-soaked gauze and stored at −20°C until testing.

2.3 Microdamage labeling, Micro-CT imaging, and Mechanical Testing

Bone marrow was removed from trabecular cores using a water pik (WP-72W, WaterPik, USA) to improve stain penetration, and one endcap was placed on the end of each sample. Trabecular cores were stained for 8 hours in 0.02% Alizarin Complex One + 10 μmol/L PI at 4°C then washed with distilled water for 1 hour to label pre-existing damage, encompassing either *in vivo* damage or damage occurring from the core extraction. The ends of the trabecular cores were glued into 5 mm deep stainless-steel endcaps to minimize end artifact effects in the mechanical test. [17] Samples were imaged with micro-computed tomography (μ-CT; μCT 40, Scanco Medical, Basserdorf, Switzerland) at a voxel resolution of 20 μm prior to mechanical testing. Trabecular cores were then mechanically tested, in which they were first preconditioned for 3 cycles to 0.1% strain then loaded in displacement-controlled uniaxial compression (Mini Bionix 858, MTS Corp.) at a rate of 0.5% strain/second to the yield strain (determined to be 1.2% in preliminary testing) and held for 3 hours. The apparent strain was calculated using a gauge length of the exposed length of the bone measured with digital calipers plus half the length of each bone end embedded in endcaps. [18] Throughout testing, bone cores were immersed in 0.9% physiological saline + 10 μmol/L PI.

After testing, one endcap was removed with the diamond saw to improve stain penetration, and cores were stained with 0.01% calcein to label test-induced microdamage for 8 hours at 4°C then washed with distilled water for 1 hour. [19,20] After staining, cores were fixed in 70% ethanol for 24 hours then dehydrated using a graded alcohol infiltration procedure. Cores were embedded in methyl methacrylate in a prescribed orientation which allowed visual registration with the 3D reconstructed μ-CT image, and 6 slides of thickness 150 μm were obtained along the longitudinal axis with the diamond saw from each sample.

2.4 Microdamage Identification and Classification

Test-induced microdamage was identified based on the criteria that cracks are intermediate in size (20 – 150 μm; larger than canaliculi but smaller than vascular channels), have sharp borders, and a focus plane demonstrating depth of field. [5,6] Areas of diffuse staining with no clearly defined cracks were not counted as microdamage. A classification system published by Moore and Gibson was modified to group damage into three broad morphological categories: severe, linear, and diffuse damage (Figure 1). [13] Severe damage was classified as either microdamage consisting of one primary crack with minor secondary cracks or cracks propagating through the thickness of the trabecula. Linear damage included both single and parallel cracks, and diffuse damage consisted of cross-hatch damage that was either equal in length and intensity (to distinguish it from severe damage) or damage with a large area of distribution.

Damage was observed at 100× magnification using fluorescence microscopy and quantified by an investigator blinded to the treatment group, then re-evaluated by a second investigator also blinded to the treatment group. A 70% concordance rate in the number of damage events identified between each investigatior was obtained, with the highest concordance rate being in the severe group (88%), and the lowest concordance rate being in the linear damage group (60%). Any differences in the count were reconciled between the two investigators, so that the total damage count is confirmed by both investigators. An area of interest for damage analysis was generated on each slide by excluding tissue less than 500 μm from each sample edge. Damage incidents demonstrating three staining patterns were counted and normalized by surface area (crack density, #/mm2). A damage incident is defined as a discrete damage event, so that both linear and diffuse damage occurrences as classified by Figure 1 would each count as one damage event. The three patterns of staining were 1) those which fluoresced predominantly under red epifluorescence corresponding to the emission

wavelength of alizarin, 2) those which fluoresced predominantly under green epifluorescence corresponding to the emission wavelength of calcein, and 3) those which fluoresced under both red and green epifluorescence equally in intensity and location.

2.5 Micro-CT Image Processing and Finite Element Analysis

3D micro-CT reconstructions of trabecular bone cores were thresholded to distinguish bone from background, and automated distance transformation algorithms were used to compute morphological parameters such as bone volume fraction, trabecular thickness and connectivity, structural model index (SMI), and degree of anisotropy (DA). Mineralization values were computed from attenuation values of grayscale μ-CT images based on hydroxyapatite (HA) calibration standards.

Micro-CT images were used to create 3-D high-resolution finite element (FE) models for estimating local stress distributions (FEA software, Scanco Medical, Basserdorf, Switzerland). A homogeneous, linear elastic, isotropic model was used, and an initial tissue modulus of 10 GPa and a Poisson ratio of 0.3 were assumed. Using Scanco software, individual damaged and undamaged trabeculae identified first during histological microdamage categorization were extracted from the 3-D reconstructed μ-CT image manually (Table 1). By manually delineating trabeculae from the reconstructed μ-CT image rather than the FEM estimation of stress distribution, the invetigators were not influenced by the stress predictions when determining cutoff points. Values for von Mises stress along the extracted trabeculae were obtained by averaging the values of all elements from the FEM solution corresponding to the voxels of the extracted trabeculae (Figure 1). Stress results were scaled to the back-calculated tissue modulus using a previously published procedure. [21] Briefly, the apparent modulus obtained from mechanical testing within the elastic region is compared to the predicted apparent modulus computed from finite element models which used an initial estimate of the trabecular tissue modulus (10 GPa). The ratio of the apparent modulus obtained from mechanical testing and predicted by finite element is multiplied by the initial estimate of the tissue modulus to obtain the effective tissue modulus based on mechanical testing results.

2.6 Statistics

All statistical tests were performed using MINITAB software (Minitab, Minitab Inc., USA). Differences in global architectural parameters between the two treatment groups and the control group were deduced using Kruskal-Wallis nonparametric tests. Differences in crack density were determined with ANOVA analysis followed by Tukey pairwise comparisons. $p<0.05$ was considered significant.

To determine differences in mechanical and architectural parameters of damaged and undamaged trabeculae by treatment group and microdamage category, Friedman's statistical test was conducted for the treatment groups and the four damage categories. Kruskal-Wallis nonparametric tests were used to determine differences between damage categories within each treatment group, followed by post-hoc nonparametric pairwise comparisons. A Bonferroni correction was used, as five measures (von Mises stress, mineralization, trabecular thickness, SMI, and trabecular orientation) were made on each analyzed trabeculae. This reduced the p value for a significant difference to $p\leq0.01$. All data are presented as mean ± standard error.

3. Results

Comparisons of alendronate's effect on the global properties of trabecular bone are shown in Table 2. Alendronate-treated trabecular bone exhibited trends towards increased bone

volume fraction, mineralization, trabecular thickness, trabecular number, and connectivity density, though none of these differences were significantly different than controls. There were no significant differences between the apparent moduli obtained during mechanical testing of alendronate samples compared to controls, nor were there differences in the back-calculated tissue moduli of alendronate-treated samples compared to controls. No dose-dependent differences in apparent properties were noted.

Figure 2 shows the crack density separated out as those cracks that were either alizarin or calcein stained only, cracks exhibiting overlapping fluorescence, and total damage (all cracks independent of color). There was a significantly higher density of calcein-labeled cracks in the control group (0.74 ± 0.03 incidents/mm^2) compared with the 0.2 mg/kg/day treatment group (0.43 ± 0.07 incidents/mm^2, $p<0.05$). Similarly, the crack density for cracks which exhibited overlapping stains was increased in the control group (0.74 ± 0.03 incidents/mm^2) compared with the 0.2 mg/kg/day treatment group (0.22 ± 0.05 incidents/mm^2). No significant differences in crack density were seen for alizarin-labeled cracks or in total damage.

In order to determine the effects of alendronate treatment on tissue level biomechanical properties, trabecular level von Mises stresses were compared to controls at microdamaged sites. As shown in Figure 3, severely damaged trabeculae in the control group were under the greatest von Mises stress, significantly greater than severely damaged trabeculae in both of the alendronate treatment groups ($p<0.001$). A treatment effect was also discerned in the linearly damaged group, where the von Mises stress state of the linearly damaged control group was significantly greater than both alendronate treatment groups ($p<0.01$).

The stress state of trabeculae exhibiting different damage morphologies were also compared within each treatment group. Severely damaged trabeculae in the control group were under significantly greater stress than all other damage morphologies in the same group ($p<0.01$). In both alendronate treatment groups, severely damage trabeculae were under greater stress than linear and undamaged trabeculae in the same group ($p<0.01$). Finally, diffusely damaged trabeculae in the ALN1.0 treatment group were under significantly greater stress than linear and undamaged trabeculae in that group ($p<0.01$).

Alterations in local mineral density were analyzed by treatment group and damage morphology. No differences due to dosage were observed, so the two treatment groups were combined. Diffusely damaged trabeculae were significantly more mineralized in bone treated with alendronate compared to controls ($p<0.01$). Similarly, undamaged trabeculae were significantly more mineralized in treated compared with untreated controls ($p<0.001$). Within the treated group, severely damaged trabeculae were less mineralized than undamaged trabeculae ($p<0.01$, Figure 4a).

To determine whether trabecular architectural characteristics were associated with damage morphology, trabecular thickness, structural model index, and trabecular alignment were computed for each extracted trabecula undergoing stress analysis. No differences in any of these architectural parameters were found between the two alendronate treatment doses; thus, the data were pooled and compared to controls. Severely damaged trabeculae were thinner than trabeculae sustaining other damage types in alendronate-treated samples ($p<0.01$, Figure 4b); this was not true for the control group. Analysis of the SMI values for damaged trabeculae revealed that severely damaged trabeculae subjected to alendronate treatment were more rod-like than their diffusely damaged counterparts ($p<0.01$, Figure 4c). Finally, the trabecular orientation, computed as the angle between the material axis and the loading axis, was significantly more acute in severely damaged trabeculae compared to undamaged trabeculae of the treated group ($p<0.01$). Severely, linearly, and diffusely

damaged trabeculae were also more aligned with the loading axis compared with undamaged trabeculae from the control group ($p<0.01$, Figure 4d).

4. Discussion

In this paper, a novel method of determining tissue-level mechanical and architectural parameters associated with microdamage morphology was used to assess the effects of alendronate on trabecular bone microstructure. Many studies have inferred that trabecular von Mises stresses increase with damage severity, but this is the first study that quantifies microstructural stresses by damage morphology. [13,22] This study concludes that alendronate administration alters the tissue level biomechanical properties of trabecular bone, resulting in a decreased von Mises stress necessary for initiation of severe and linear microdamage.

Many previously published studies have utilized the fluorescent staining protocol developed by O'Brien *et al*. to separate *in vivo* damage from test-induced damage. [20,23,24] In our execution of this protocol, we were able to separate cracks formed *in vivo* from those induced during uniaxial compression loading by examining their fluorescence under green and red epifluorescence. Though total *in vivo* damage was not significantly greater in alendronate treated bone, linear crack density was significantly increased in this population, which is in agreement with previously published work. [5] However, it was difficult to determine whether cracks which fluoresced under both red and green epifluorescence equally are the product of crack propagation, double staining due to the sharing of calcium binding sites between the two fluorophores, or filter interference. Due to these difficulties, we chose to exclude cracks which exhibited this overlapping fluorescence from the stress analysis due to the uncertainty of their origins.

Previous studies have correlated microdamage formation to trabecular shear stress, suggesting that shear forces play a significant role in trabecular bone failure. [22,25,26] The contribution of shear forces to failure can be evaluated with the von Mises stress parameter, which is commonly used to predict yielding in complex loading conditions when the shear stress reaches a critical value on the octahedral plane. Fyhrie *et al* demonstrated that von Mises stress concentrations correlated with sites of cracking in mechanically tested and *in vivo* damaged trabecular bone. [25] Our findings suggest that trabecular bone treated with alendronate may be more susceptible to severe and linear microdamage formation because of a decreased von Mises stress magnitude required to induce damage compared to controls. Linear damage can reduce the biomechanical properties of bone and is traditionally associated with the terminal phase of bone fracture characterized by rapid crack propagation and catastrophic failure [10,11]; thus, alendronate administration may predispose trabecular bone to the formation of more ominous microdamage patterns in the form of severe and linear microdamage. [10,11,27] These observations may account for increased microcrack density in trabecular bone treated with alendronate for one year as more damage would form if the initiation threshold is lowered in this population. [5]

Alendronate treatment has been shown to increase the thickness and mineralization of trabeculae, and this study corroborates that finding. [28] We found that thinner trabeculae with decreased mineral density and rod-like morphology are more likely to sustain severe damage in the treated samples compared to non-treated controls. The data suggest that the vulnerability of trabeculae to damage based on thinness is relative to the average trabecular thickness of the sample, for at the thickness of alendronate-treated severely damaged trabeculae, untreated trabeculae at the same thickness were undamaged. There are two possible mechanisms to explain this finding: either there is a decrease in bone quality factors (tissue-matrix characteristics) in alendronate-treated trabeculae that promote damage

formation, or architectural changes stemming from alendronate treatment that expose the vulnerability of thinner trabeculae to damage. Since trabecular stresses in severely damaged trabeculae were actually decreased compared to control samples, indicating that architectural changes do not place greater stresses on thinner trabeculae, this suggests that some other factor(s) related to bone quality facilitates severe damage formation in alendronate-treated bone.

It is well documented that due to the suppression of bone remodeling, alendronate increases tissue mineralization. [5,29] When mineralization density was compared based on trabecular damage morphology, we found that mineralization was only increased in alendronate-treated samples which were diffusely damaged or undamaged. Severely and linearly damaged trabeculae in alendronate-treated samples were not differently mineralized compared to control trabeculae with the same damage morphology. We have previously shown that microdamage initiation occurs around areas of decreased mineralization, and speculate that regions of low mineral/matrix ratio may result in greater local tissue compliance leading to damage initiation. [30] This effect may be seen only at the 1 year stage of treatment as matrix mineral will continue to age and stiffen as bone turnover declines.

Some aspects of the present study limit its broad applicability. This study was conducted in bone from twelve animals, or four per treatment group. This limits the power of the study to resolve stress differences due to treatment dose ($1-\beta=0.49$) or global architectural changes like bone volume fraction with alendronate treatment ($1-\beta=0.34$). Our stress analysis was conducted by analyzing almost 400 trabeculae, so we are more confident in the power of the study to resolve differences in the stress state due to damage morphology ($1-\beta$ approaches 1). Also, bone used for the microdamage analysis came from non-osteoporotic animals; thus, it is difficult to apply conclusions to osteoporotic humans using bisphosphonate therapies. However, our study focused on changes in intrinsic level properties of trabecular bone elicited by alendronate use, and the bone physiology of humans and dogs is sufficiently similar to allow such investigations. [31,32] Conclusions from this study are also limited by the assumption of linearity, homogeneity, and isotropy at the microstructural level, which somewhat limits the accuracy of the mechanical values obtained. However, Nagaraja et.al. have shown that including inhomogeneous tissue moduli in finite element models offers only a modest improvement in the correlations between microdamage initiation and local stresses. Furthermore, strong correlations between stress magnitudes and damage severity argue in favor of the finite element models' accuracy in predicting tissue-level biomechanical properties. [16] Additionally, the conservative nature of the statistical tests used adds confidence to the conclusion that distinct differences in the state of stress of trabeculae bearing different microdamage to patterns exist.

In conclusion, alendronate alters local mechanical and architectural properties of trabecular bone which may increase its susceptibility to damage after just one year of treatment. This study furthers our understanding of local tissue failure mechanisms, particularly in relation to the factors influencing damage morphology formation. The clinical implications of these findings are unclear, since increased risk of fracture with long-term alendronate use has not been documented.

Acknowledgments

This study was supported by NIH grants 5R01AG027249, 5R01AR047838 and 5T32AR007581. Merck and Co. kindly provided the alendronate. The micro-CT system was provided by an NSF Major Research Instrumentation Award (9977551).

Role of the Funding Source

The NIH and NSF had no role in the collection, analysis and interpretation of data; in the writing of the report; and in the decision to submit the paper for publication. Merck and Co. reviewed the article before submission.

References

1. Seeman E. The antifracture efficacy of alendronate. Int J Clin Pract Suppl 1999;101:40–5. [PubMed: 12675021]
2. Liberman UA, Weiss SR, Broll J, Minne HW, Quan H, Bell NH, Rodriguez-Portales J, Downs RW Jr, Dequeker J, Favus M. Effect of oral alendronate on bone mineral density and the incidence of fractures in postmenopausal osteoporosis. The Alendronate Phase III Osteoporosis Treatment Study Group. N Engl J Med 1995;333(22):1437–43. [PubMed: 7477143]
3. Iwamoto J, Sato Y, Takeda T, Matsumoto H. Hip fracture protection by alendronate treatment in postmenopausal women with osteoporosis: a review of the literature. Clin Interv Aging 2008;3(3): 483–9. [PubMed: 18982918]
4. Seeman E. Is a change in bone mineral density a sensitive and specific surrogate of anti-fracture efficacy? Bone 2007;41(3):308–17. [PubMed: 17644058]
5. Allen MR, Iwata K, Phipps R, Burr DB. Alterations in canine vertebral bone turnover, microdamage accumulation, and biomechanical properties following 1-year treatment with clinical treatment doses of risedronate or alendronate. Bone 2006;39(4):872–9. [PubMed: 16765660]
6. Stepan JJ, Burr DB, Pavo I, Sipos A, Michalska D, Li J, Fahrleitner-Pammer A, Petto H, Westmore M, Michalsky D, Sato M, Dobnig H. Low bone mineral density is associated with bone microdamage accumulation in postmenopausal women with osteoporosis. Bone 2007;41(3):378–85. [PubMed: 17597017]
7. Chapurlat RD, Arlot M, Burt-Pichat B, Chavassieux P, Roux JP, Portero-Muzy N, Delmas PD. Microcrack frequency and bone remodeling in postmenopausal osteoporotic women on long-term bisphosphonates: a bone biopsy study. J Bone Miner Res 2007;22(10):1502–9. [PubMed: 17824840]
8. Wenzel TE, Schaffler MB, Fyhrie DP. In vivo trabecular microcracks in human vertebral bone. Bone 1996;19(2):89–95. [PubMed: 8853850]
9. Reilly GC, Currey JD. The effects of damage and microcracking on the impact strength of bone. J Biomech 2000;33(3):337–43. [PubMed: 10673117]
10. Diab T, Vashishth D. Effects of damage morphology on cortical bone fragility. Bone 2005;37(1): 96–102. [PubMed: 15897021]
11. Burr DB, Turner CH, Naick P, Forwood MR, Ambrosius W, Hasan MS, Pidaparti R. Does microdamage accumulation affect the mechanical properties of bone? J Biomech 1998;31(4):337–45. [PubMed: 9672087]
12. Diab T, Condon KW, Burr DB, Vashishth D. Age-related change in the damage morphology of human cortical bone and its role in bone fragility. Bone 2006;38(3):427–31. [PubMed: 16260195]
13. Arthur Moore TL, Gibson LJ. Microdamage accumulation in bovine trabecular bone in uniaxial compression. J Biomech Eng 2002;124(1):63–71. [PubMed: 11873773]
14. Wang X, Niebur GL. Microdamage propagation in trabecular bone due to changes in loading mode. J Biomech 2006;39(5):781–90. [PubMed: 16488217]
15. Nagaraja S, Couse TL, Guldberg RE. Trabecular bone microdamage and microstructural stresses under uniaxial compression. J Biomech 2005;38(4):707–16. [PubMed: 15713291]
16. Nagaraja S, Lin AS, Guldberg RE. Age-related changes in trabecular bone microdamage initiation. Bone 2007;40(4):973–80. [PubMed: 17175210]
17. Keaveny TM, Wachtel EF, Ford CM, Hayes WC. Differences between the tensile and compressive strengths of bovine tibial trabecular bone depend on modulus. J Biomech 1994;27(9):1137–46. [PubMed: 7929463]
18. Keaveny TM, Pinilla TP, Crawford RP, Kopperdahl DL, Lou A. Systematic and random errors in compression testing of trabecular bone. J Orthop Res 1997;15(1):101–10. [PubMed: 9066533]
19. Vashishth D, JC, Clovis N, Tanner KE, Bonfield W. Double staining technique for histological evaluation of microcracks in cortical bone. Proc 2nd World Cong Biomech 1994;I:44.

20. O'Brien FJ, Taylor D, Lee TC. An improved labelling technique for monitoring microcrack growth in compact bone. J Biomech 2002;35(4):523–6. [PubMed: 11934422]
21. van Rietbergen BWH, Huiskes R, Odgaard A. A new method to determine trabecular bone elastic properties and loading using micromechanical finite-element models. J Biomech 1995;28(1):69–81. [PubMed: 7852443]
22. Yeni YN, Hou FJ, Ciarelli T, Vashishth D, Fyhrie DP. Trabecular shear stresses predict in vivo linear microcrack density but not diffuse damage in human vertebral cancellous bone. Ann Biomed Eng 2003;31(6):726–32. [PubMed: 12797623]
23. Wang X, Guyette J, Liu X, Roeder RK, Niebur GL. Axial-shear interaction effects on microdamage in bovine tibial trabecular bone. Eur J Morphol 2005;42(1–2):61–70. [PubMed: 16123025]
24. Zarrinkalam KH, Kuliwaba JS, Martin RB, Wallwork MA, Fazzalari NL. New insights into the propagation of fatigue damage in cortical bone using confocal microscopy and chelating fluorochromes. Eur J Morphol 2005;42(1–2):81–90. [PubMed: 16123027]
25. Fyhrie DP, Hoshaw SJ, Hamid MS, Hou FJ. Shear stress distribution in the trabeculae of human vertebral bone. Ann Biomed Eng 2000;28(10):1194–9. [PubMed: 11144980]
26. Yeni YN, Zelman EA, Divine GW, Kim DG, Fyhrie DP. Trabecular shear stress amplification and variability in human vertebral cancellous bone: relationship with age, gender, spine level and trabecular architecture. Bone 2008;42(3):591–6. [PubMed: 18180212]
27. Burr DB, Forwood MR, Fyhrie DP, Martin RB, Schaffler MB, Turner CH. Bone microdamage and skeletal fragility in osteoporotic and stress fractures. J Bone Miner Res 1997;12(1):6–15. [PubMed: 9240720]
28. Recker R, Masarachia P, Santora A, Howard T, Chavassieux P, Arlot M, Rodan G, Wehren L, Kimmel D. Trabecular bone microarchitecture after alendronate treatment of osteoporotic women. Curr Med Res Opin 2005;21(2):185–94. [PubMed: 15801989]
29. Allen MR, Burr DB. Mineralization, Microdamage, and Matrix: How Bisphosphonates Influence Material Properties of Bone. BoneKEy-Osteovision 2007;4(2):49–60.
30. Nagaraja, SONJM.; Boskey, A.; Guldberg, RE. Age-Related Alterations in Mineral/Matrix Ratio in Test-induced Microdamaged Trabeculae. ORS 55th Annual Meeting; 2009.
31. Aerssens J, Boonen S, Lowet G, Dequeker J. Interspecies differences in bone composition, density, and quality: potential implications for in vivo bone research. Endocrinology 1998;139(2):663–70. [PubMed: 9449639]
32. Shaw JAW, Scott C, Bruno Anthony, Paul Emmanuel M. Comparison of primate and canine models for bone ingrowth experimentation, with reference to the effect of ovarian function on bone ingrowth potential. Journal of Orthopaedic Research 2005;12(2):268–273. [PubMed: 8164101]

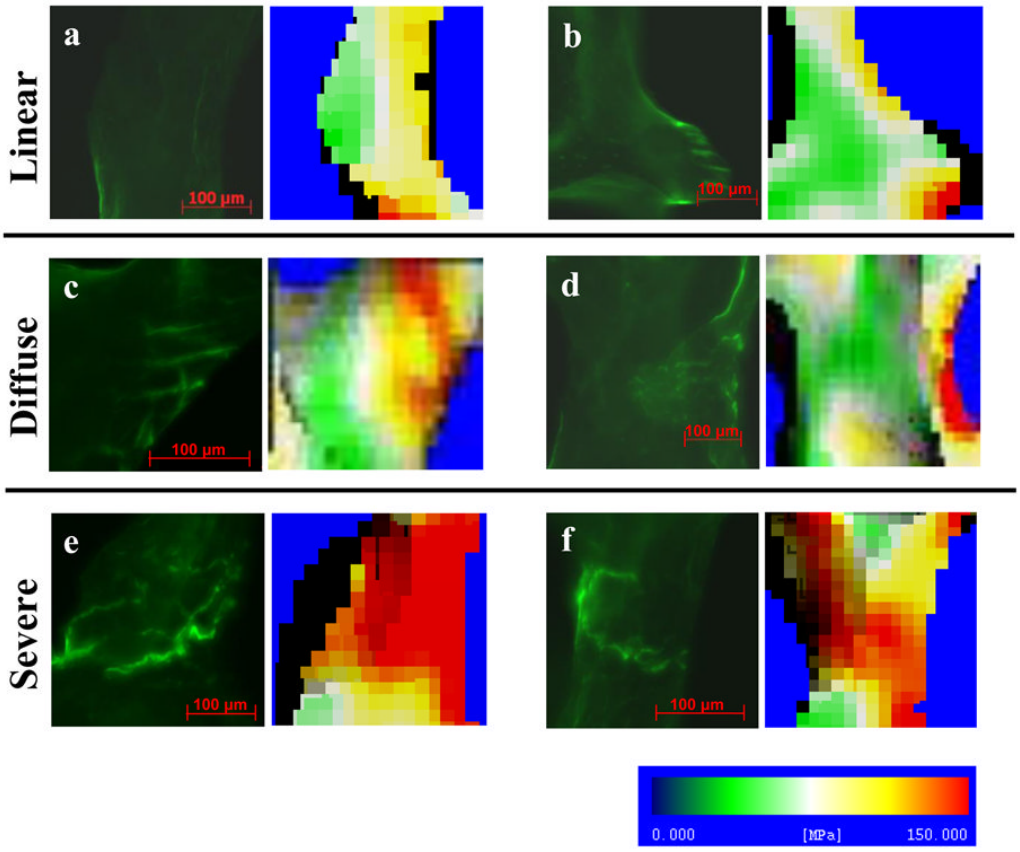

Figure 1.
Microdamage description and classification, with FEA von Mises stress predictions. *i.* Linear damage including a) single crack and b) parallel cracks, *ii*. Diffuse (crosshatch) damage including c) equal crosshatching and d) large area distribution, *iii*. Severe damage including e) one primary crack with minor secondary cracks and f) through-thickness cracks.

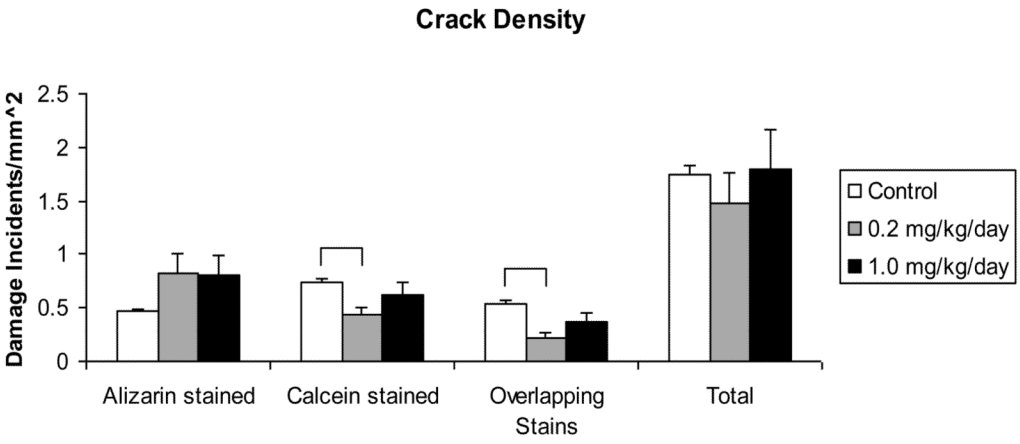

Figure 2.

Total damage quantified based on fluorescence and plotted by treatment group. An increased amount of damage occurred due to the mechanical test in the control group. The total damage columns are created by totaling damage counted in the three previous columns for each treatment group, and no significant differences were found. Bars represent significant differences. $p<0.05$, mean ± SE. is plotted

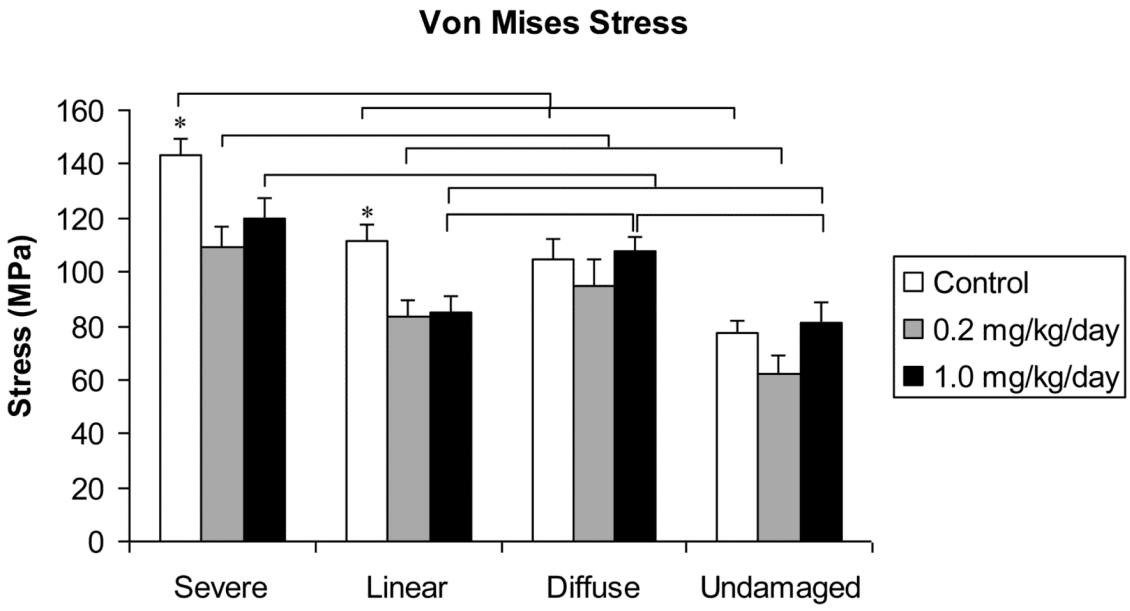

Figure 3.

Von Mises stress plotted by treatment group and damage morphology. The stress state of trabeculae exhibiting severe and linear damage was decreased in both treatment groups compared with controls. In the control group, severe damage was associated with the greatest stress compared with all other damage groups. In both treatment groups, the stress state of severely damaged trabeculae was significantly increased compared with linear and undamaged trabeculae. Bars between damage morphologies within the same treatment group indicate significant differences. $p<0.01$ indicates significance, mean + SE is plotted.

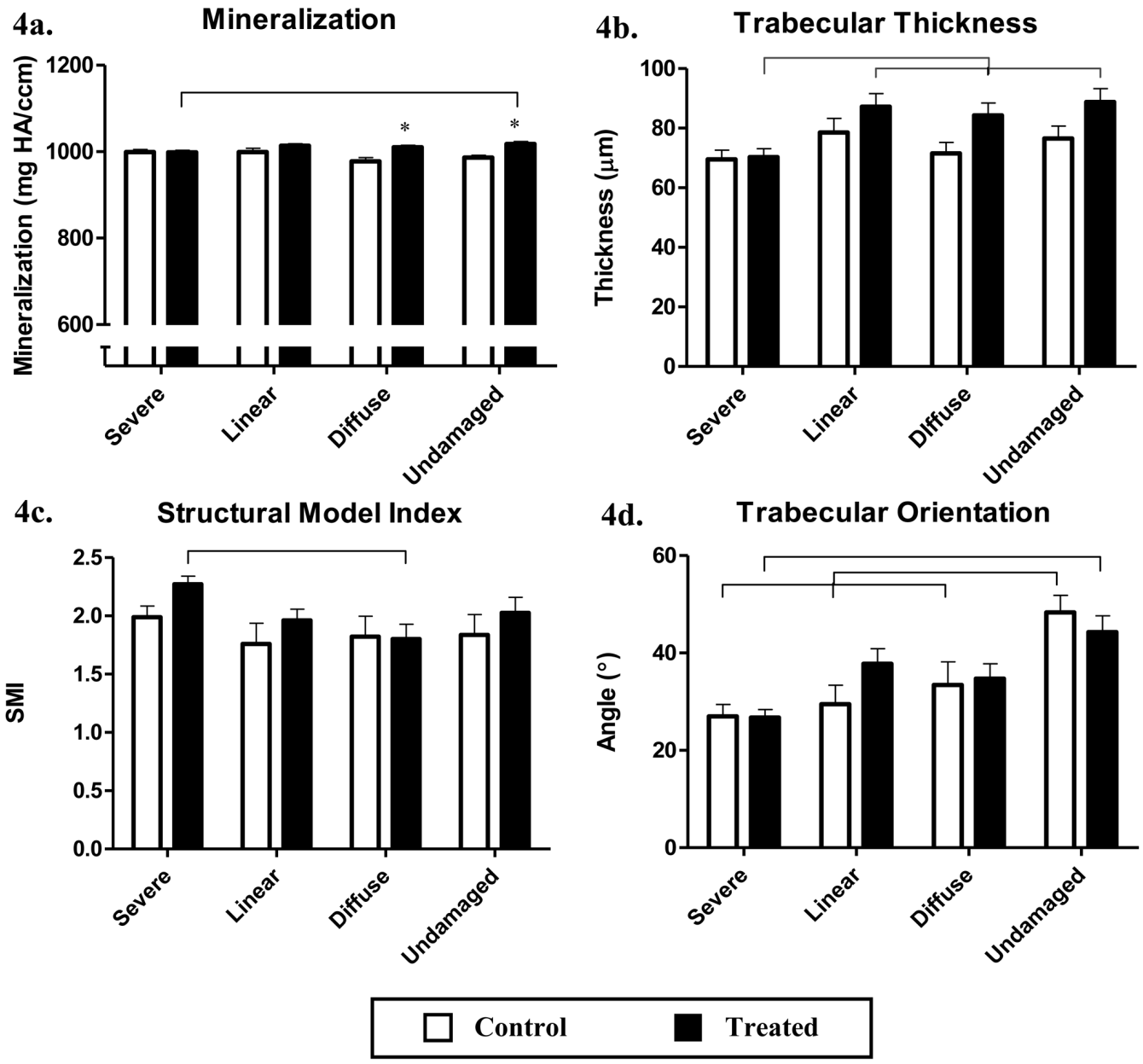

Figure 4.

Trabecular mineralization and architectural characteristics plotted by treatment group and damage morphology. There were no differences due to treatment dose, so the two samples were combined. **4a.** Trabecular mineralization is plotted with respect to damage morphology and treatment; severely damaged trabeculae were less mineralized than undamaged trabeculae in the treated group. **4b.** Trabecular thickness is plotted with respect to treatment and damage morphology; severely damaged trabeculae were significantly thinner than other trabeculae in the treated group. **4c.** Structural model index is plotted with respect to damage morphology and treatment; severely damaged trabeculae are more rod-like than diffusely damaged trabeculae. **4d.** The angle between the principal material axis and the loading axis is plotted; undamaged trabeculae were generally aligned perpendicular to the loading axis in both treatment and control groups*indicates a significantly increased angle compared with all other damage morphologies in the same group. Bars indicate significant differences

between damage morphologies within the same group. $p<0.01$ indicates significance, mean + SE plotted

Table 1

Sample Sizes for Trabecular Stress Analysis by Treatment Group and Damage Morphology

	Severe	Linear	Diffuse	Undamaged	Total
Control	62	26	31	35	154
0.2 mg/kg/day	28	31	25	19	103
1.0 mg/kg/day	49	25	30	31	135

These trabeculae exhibited damage which fluoresced under green epifluorescence only. Undamaged trabeculae showed no fluorescence under either red or green epifluorescence.

Table 2

Apparent Properties of Alendronate-treated and Control Samples

	0.2 mg/kg/day	**1.0 mg/kg/day**	**Control**
Bone Volume Fraction (BV/TV)	0.20 ± 0.01	0.19 ± 0.007	0.13 ± 0.007
Mineralization (mg HA/ccm)	1040.3 ± 6.1	1040.3 ± 1.0	1011.9 ± 6.2
Trabecular Thickness (μm)	107.8 ± 5.4	106.7 ± 2.6	87.8 ± 2.3
Connectivity Density	24.5 ± 1.2	25.2 ± 1.2	18.7 ± 1.4
Structural Model Index (SMI)	1.12 ± 0.08	1.33 ± 0.04	1.43 ± 0.06
Degree of Anisotropy	1.43 ± 0.02	1.31 ± 0.02	1.41 ± 0.04
Trabecular Number	2.25 ± 0.04	2.21 ± 0.05	2.06 ± 0.05
Apparent Modulus (MPa)	872.7 ± 71.0	825.2 ± 57.6	600.0 ± 73.5
Tissue Modulus (GPa)	12.3 ± 1.9	13.1 ± 2.2	14.7 ± 1.1

No significant differences were noted.